

Winter Atmospheric Circulation Anomaly Associated with Recent Arctic Winter Warm Anomalies

BINGYI WU

Institute of Atmospheric Sciences, Fudan University, Shanghai, and Chinese Academy of Meteorological Sciences, Beijing, China

(Manuscript received 17 March 2017, in final form 22 June 2017)


ABSTRACT

The winter Arctic atmosphere in the middle and lower troposphere has shifted to a warmer stage since the winter of 2004/05 relative to the mean averaged from 1979/80 to 2003/04. Recent Arctic warm anomalies are concurrent with warm anomalies over the North Pacific, northern Africa, and the low latitudes of both the North American and Asian continents and with cold anomalies over the middle and high latitudes of Eurasia and North America. Meanwhile, strengthened winter SLP is observed in the middle and high latitudes of Eurasia, the Siberian marginal seas of the Arctic Ocean, and the North Pacific. Correspondingly, winter 500-hPa geopotential height anomalies exhibit wave train structures over Eurasia, the North Pacific, and North America. These major features frequently reappear since the winter of 2004/05. A regionally averaged winter SLP in 40°–65°N, 30°E–150°W can be regarded as the intensity index to characterize interannual variability of the atmospheric circulation anomaly associated with recent Arctic warm anomalies. This atmospheric circulation anomaly differs from the Arctic dipole anomaly and displays a closer association with atmospheric variability over the middle and low latitudes relative to the Arctic. It directly connects Arctic warm anomalies in the middle and lower troposphere to increased frequencies of extreme cold events in the middle and low latitudes of Eurasia and western North Pacific, and western North America. This study also implies that SST cooling in the tropical central and eastern Pacific may also contribute to recent Arctic warm anomalies, although its impact mechanism is not clear yet.

1. Introduction

The Arctic is a key area in discussion on climate variability and change because of its sensitivity to global warming and its possible influence on weather and climate in the middle and lower latitudes (Screen and Simmonds 2010; Francis and Vavrus 2012, 2015; Cohen 2016; Overland and Wang 2010; Overland et al. 2011, 2016; Semenov and Latif 2015). The surface warming in the Arctic is 2–3 times faster than the global average (Serreze and Barry 2011; Andry et al. 2017); this is referred to as Arctic amplification (AA). Many studies have investigated possible influences of AA and melting sea ice on weather and climate in the midlatitudes (Francis and Vavrus 2012, 2015; Screen and Simmonds

2013; Cohen et al. 2012, 2014; Cohen 2016; Jaiser et al. 2012; Vihma 2014; Wu et al. 2013a,b; and many others) although their associations exhibit some uncertainties and the linking mechanisms still are an ongoing debate (Barnes 2013; Wallace et al. 2014; Barnes and Screen 2015; Petoukhov and Semenov 2010; Screen et al. 2014; Walsh 2014; Jung et al. 2015; Overland et al. 2015, 2016; Perlwitz et al. 2015; Semenov and Latif 2015; Wu et al. 2015; Sun et al. 2016). In fact, differences in location and strength of Arctic warm anomalies in the middle and lower troposphere could affect the meridional thermal gradient and zonal winds, resulting in different effects on weather and climate. Kug et al. (2015) emphasized the roles of surface air temperature (SAT) anomalies and showed that cold winters across East Asia are associated with warm anomalies in the Barents–Kara Seas, whereas severe winters in North America are linked to warm anomalies in the East Siberian and Chukchi Seas. On the other hand, thermal conditions in the middle and low latitudes also play a role in resulting thermal gradients, which is one of reasons for the uncertainty of

 Denotes content that is immediately available upon publication as open access.

Corresponding author: Bingyi Wu, bywu@fudan.edu.cn

DOI: 10.1175/JCLI-D-17-0175.1

© 2017 American Meteorological Society. For information regarding reuse of this content and general copyright information, consult the [AMS Copyright Policy](http://www.ametsoc.org/PUBSReuseLicenses) (www.ametsoc.org/PUBSReuseLicenses).

linkages between the Arctic and the middle and low latitudes.

The Arctic SATs are generally used to characterize Arctic warming and AA. However, SATs are strongly influenced by the external forcing, such as sea ice concentrations (SICs) and surface sea temperatures (SSTs). Thus differences in SATs between the Arctic and the midlatitudes may exaggerate the thermal contrast of atmospheric circulation in the middle and lower troposphere. The updated study also indicated that warming in the lower troposphere associated with AA is not a direct driver of anomalous midlatitude atmospheric circulation changes (Sellevold et al. 2016). Consequently, it is necessary to investigate dominant features of vertically averaged air temperature in the middle and lower troposphere in the Arctic and its association with atmospheric circulation variability. Revealing the dominant features of winter atmospheric variability that are closely associated with Arctic warm anomalies in the middle and lower troposphere rather than Arctic SAT anomalies would be helpful for comprehensively understanding the linkage between Arctic warm anomalies and the midlatitude climate variability. This is the motivation of the present study.

2. Data and methods

In this study, the atmospheric data, including the monthly mean sea level pressure (SLP), SATs, and geopotential heights from January 1979 to February 2016 and daily SATs from 1 January 1979 to 28 February 2016 are obtained from the NCEP–NCAR reanalysis (see <http://iridl.ldeo.columbia.edu/SOURCES/NOAA/NCEP-NCAR/CDAS-1/>). Daily SATs are used to calculate occurrence frequency of extreme cold events when daily SATs are below negative one standard deviation. This study also used the monthly mean Eurasian (or east Atlantic/western Russia) pattern and the Pacific–North American (PNA) pattern indices (taken from <http://www.cpc.ncep.noaa.gov/data/teledoc/telecontents.shtml>). The Siberian high index (SHI) is defined as a regionally averaged winter SLP over the domain 40° – 60° N, 80° – 120° E (Wu and Wang 2002). This study also used the following datasets: 1) the SIC dataset ($1^{\circ} \times 1^{\circ}$) from January 1979 to May 2016, obtained from the British Atmospheric Data Centre (BADC; Hadley Centre for Climate Prediction and Research 2006) and 2) a monthly mean SST dataset ($2^{\circ} \times 2^{\circ}$) from 1979 to 2015 (see <http://rda.ucar.edu/datasets/ds277.0/>; Smith and Reynolds 2003). The monthly Pacific decadal oscillation (PDO) index and Niño-3.4 index from 1979 to 2016 are respectively taken from <http://research.jisao.washington.edu/pdo/PDO.latest.txt> and <http://www.cpc.ncep.noaa.gov/data/indices/>.

This study uses winter (December–February) mean 1000–500-hPa atmospheric thickness to approximately

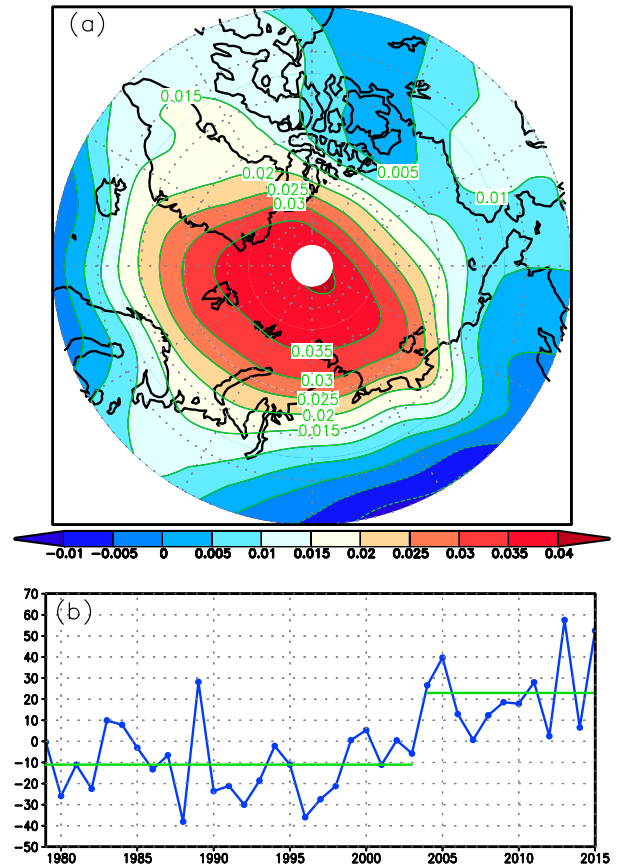


FIG. 1. (a) The spatial distribution of the leading EOF of winter 1000–500-hPa atmospheric thickness variability north of 60° N and (b) its principal component time series (blue line); the green lines represent the winter means averaged over 1979/80–2003/04 and 2004/05–2015/16.

represent a vertical averaged air temperature in the middle and lower troposphere, and the empirical orthogonal function (EOF) analysis method is applied to extract dominant features of winter mean 1000–500-hPa atmospheric thickness variability.

3. Results

a. Dominant features of recent Arctic winter warm anomalies and their association with atmospheric circulation anomalies

To extract dominant features of Arctic winter mean air temperature in the middle and lower troposphere, EOF analysis is performed for winter mean 1000–500-hPa atmospheric thickness variability. The leading EOF of atmospheric thickness variability north of 60° N accounts for 31% of the total variance. Spatially, positive anomalies cover most parts of the Arctic Ocean and its marginal seas; the center of this area is close to the Nordic seas and the Barents Sea (Fig. 1a). The leading

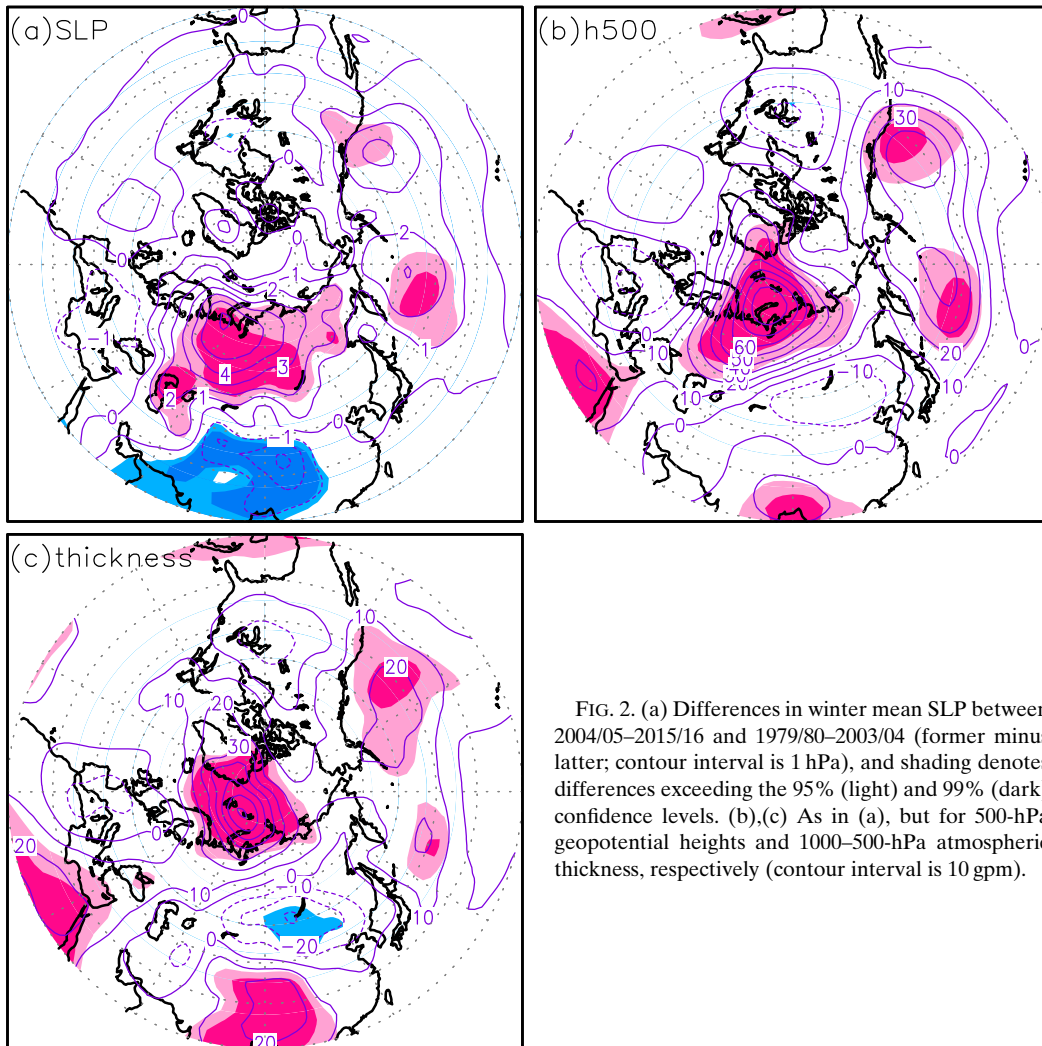


FIG. 2. (a) Differences in winter mean SLP between 2004/05–2015/16 and 1979/80–2003/04 (former minus latter; contour interval is 1 hPa), and shading denotes differences exceeding the 95% (light) and 99% (dark) confidence levels. (b),(c) As in (a), but for 500-hPa geopotential heights and 1000–500-hPa atmospheric thickness, respectively (contour interval is 10 gpm).

principal component experienced a “jump” after the winter of 2003/04, indicating that the Arctic has shifted to a warmer stage relative to before the winter of 2004/05 (Fig. 1b). A similar phenomenon also was observed in the leading EOF of winter mean 1000–500-hPa thickness (not shown) and SAT variability of the reanalysis data from ERA-Interim (see Fig. 1 of Feng and Wu 2015).

Figure 2 shows differences in winter mean variables between 2004/05–2015/16 and 1992/93–2003/04, which reflects winter atmospheric changes being associated with Arctic winter warm anomalies. Positive SLP anomalies occupied the middle and high latitudes of Eurasia, the Siberian marginal seas of the Arctic Ocean, and the North Pacific (Fig. 2a). Meanwhile, deepened winter SLP is observed in the middle and lower latitudes of Asia. The 500-hPa geopotential height anomalies show a wave train structure over Eurasia and the Arctic, with a dominant positive center over the Barents–Kara

Seas and two separated negative centers over East Asia and the Mediterranean region (Fig. 2b). Additionally, positive 500-hPa geopotential height anomalies also appear over the North Pacific, with negative anomalies over the central and eastern North America. Significant positive height anomalies also emerge over the low latitudes of Africa and the Asian continent. At the 1000–500-hPa thickness field, in the middle and high latitudes, there are two anomalous warm regions (thickness anomalies >20 gpm): one is from northeastern Canada across Greenland extending northeastward into the Laptev Sea and other is the North Pacific (Fig. 2c). Additionally, two separated positive centers are observed over northern Africa and the Asian continent south of 40°N . On the contrary, anomalous cold regions mainly emerge in western Europe and the middle and high latitudes of Asia and North America. These dominant features in winter SLP and 1000–500-hPa thickness

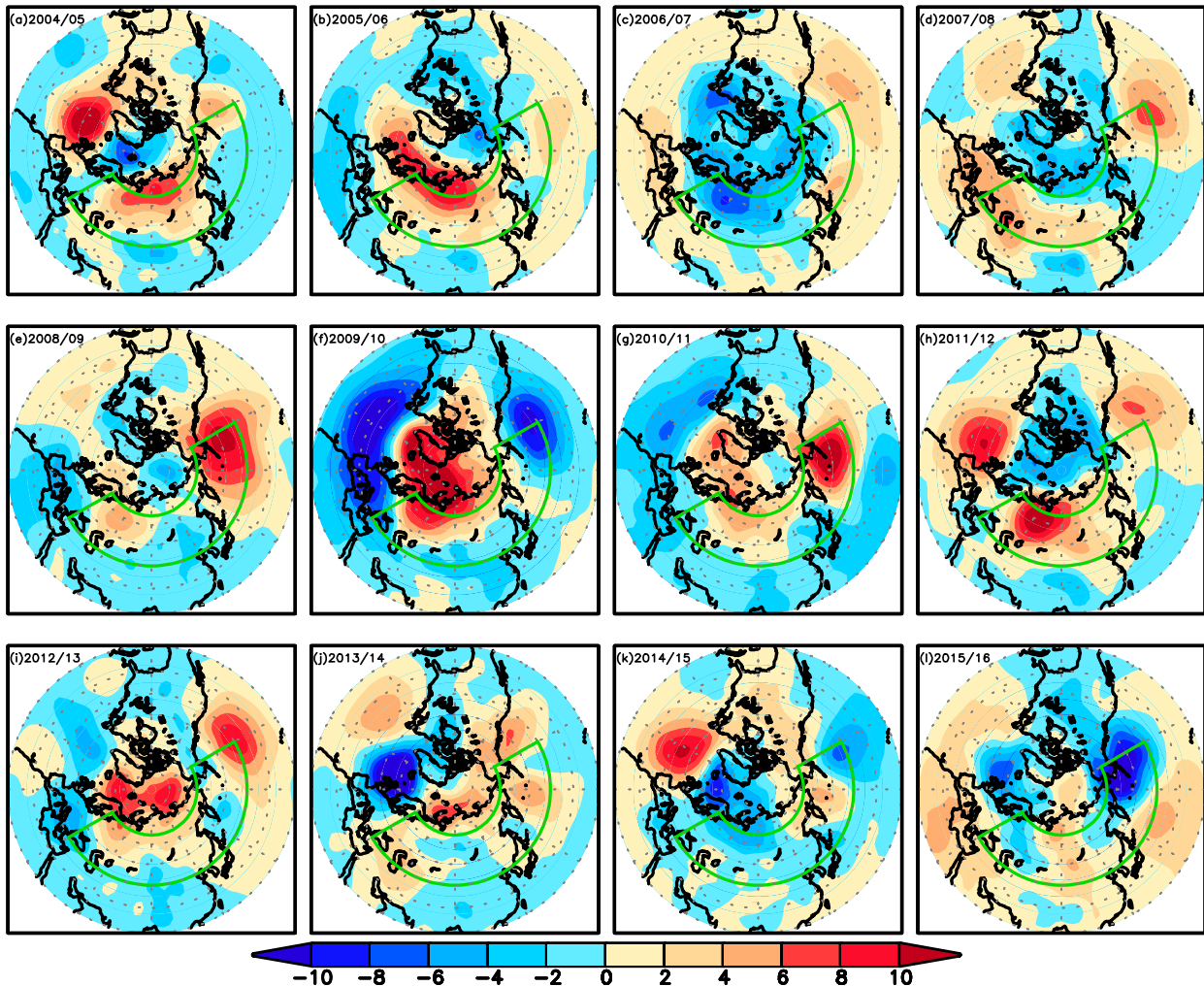


FIG. 3. Winter mean SLP anomalies (relative to the winter mean averaged over 1979/80–2015/16) in each winter since 2004 (contour interval is 2 hPa), and the area outlined in green (40° – 65° N, 30° E– 150° W) is selected to calculate the intensity index of the atmospheric circulation anomaly.

anomalies, to some extent, are also detectable in each winter since 2004. It is found that there were 8 of 12 winters showing a dominant feature that positive SLP anomalies appeared simultaneously in the northern Eurasian/Siberian marginal seas and the North Pacific, including the winters of 2004/05, 2005/06, 2007/08, 2008/09, 2010/11, 2011/12, 2012/13, and 2013/14 (Figs. 3a–l). This implies that since 2004 Arctic winter warm anomalies in the middle and lower troposphere, to a great extent, have been concurrent with raised SLP in the middle and high latitudes from northern Eurasia to the North Pacific. At 1000–500-hPa thickness fields, there were 9 of 12 winters satisfying the condition that Arctic warm anomalies are accompanied by warm anomalies over the North Pacific: the winters of 2004/05, 2005/06, 2007/08, 2008/09, 2009/10, 2010/11, 2011/12, 2012/13, and

2013/14 (Figs. 4a–l). Thus, since 2004 there have been only three winters (2006/07, 2014/15, and 2015/16) that did not display the dominant features shown in Fig. 2.

A further analysis shows that a regionally averaged SLP over the domain 40° – 65° N, 30° E– 150° W can be regarded as the intensity index to characterize interannual variability of the atmospheric circulation anomaly associated with recent Arctic winter warm anomalies. Spatial distributions of atmospheric circulation anomalies in Figs. 5a–c closely resemble those in Figs. 2a–c except for the North Pacific where a monopole structure replaces two separated anomalous centers. Significant positive SLP anomalies are observed in the middle and high latitudes of Eurasia and the North Pacific, and there are two positive centers respectively over the area around the Ural Mountains and over the

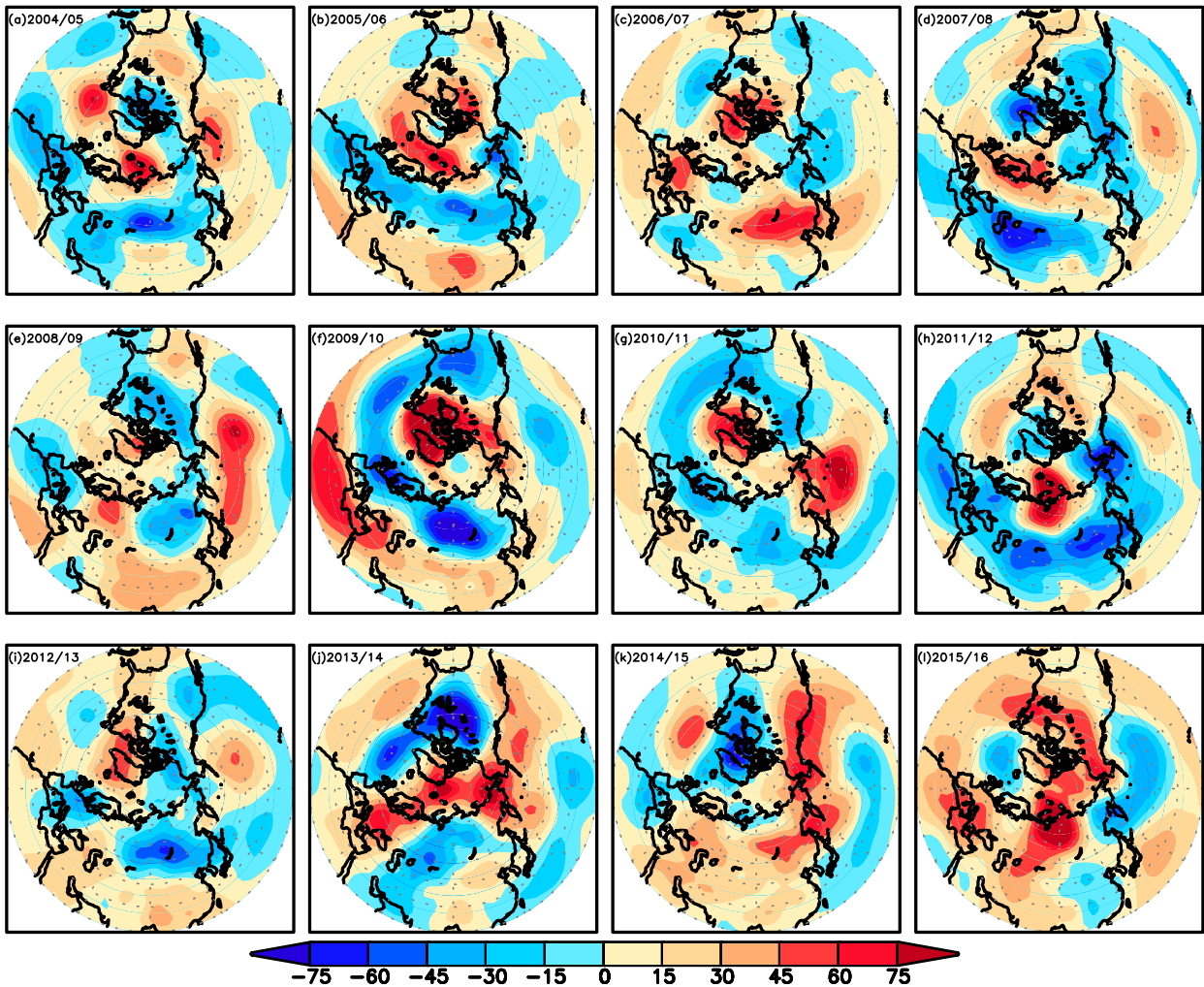


FIG. 4. Winter mean 1000–500-hPa thickness anomalies (relative to the winter mean averaged over 1979/80–2015/16) in each winter since 2004 (contour interval is 15 gpm).

northern North Pacific close to the Aleutian Islands (Fig. 5a). Significant negative SLP anomalies emerge in the middle and low latitudes from Africa eastward to the central Pacific. At 500 hPa, geopotential height anomalies display a tripole structure over Eurasia and the Arctic (Fig. 5b). Significant positive height anomalies occupy the North Pacific and negative anomalies appear in the middle and high latitudes of Eurasia and central and eastern North America. At the 1000–500-hPa thickness field, warm anomalies in the Arctic and the North Pacific are concurrent with cold anomalies in the middle and high latitudes of Eurasia and North America (Fig. 5c). Additionally, cold anomalies also emerge in the low latitudes of the Pacific. This atmospheric circulation anomaly also experienced a jump after the winter of 2003/04 (Fig. 6), consistent with the evolution of Arctic atmospheric thickness variability. In the last two

winters, however, it returned to the status before the winter of 2004/05, differing from the evolution of Arctic atmospheric thickness variability (Fig. 1b).

This atmospheric circulation anomaly clearly differs from the anomalous pattern associated with winter SAT anomalies in the Barents–Kara Seas (Figs. 5d–f). When winter SAT anomalies are positive in the Barents–Kara Seas, corresponding SLP anomalies exhibit a dipole structure in the middle and high latitudes of Eurasia and the Arctic, with opposing anomalous centers respectively over northern Eurasia and between the Arctic Ocean and the Nordic seas (Fig. 5d). Meanwhile, anomalies in both of SLP and 500-hPa geopotential heights do not exceed any significant level over the North Pacific (Figs. 5d,e). Over the Bering Sea, there is a smaller area where the 1000–500-hPa thickness exhibits significant negative anomalies, rather than positive

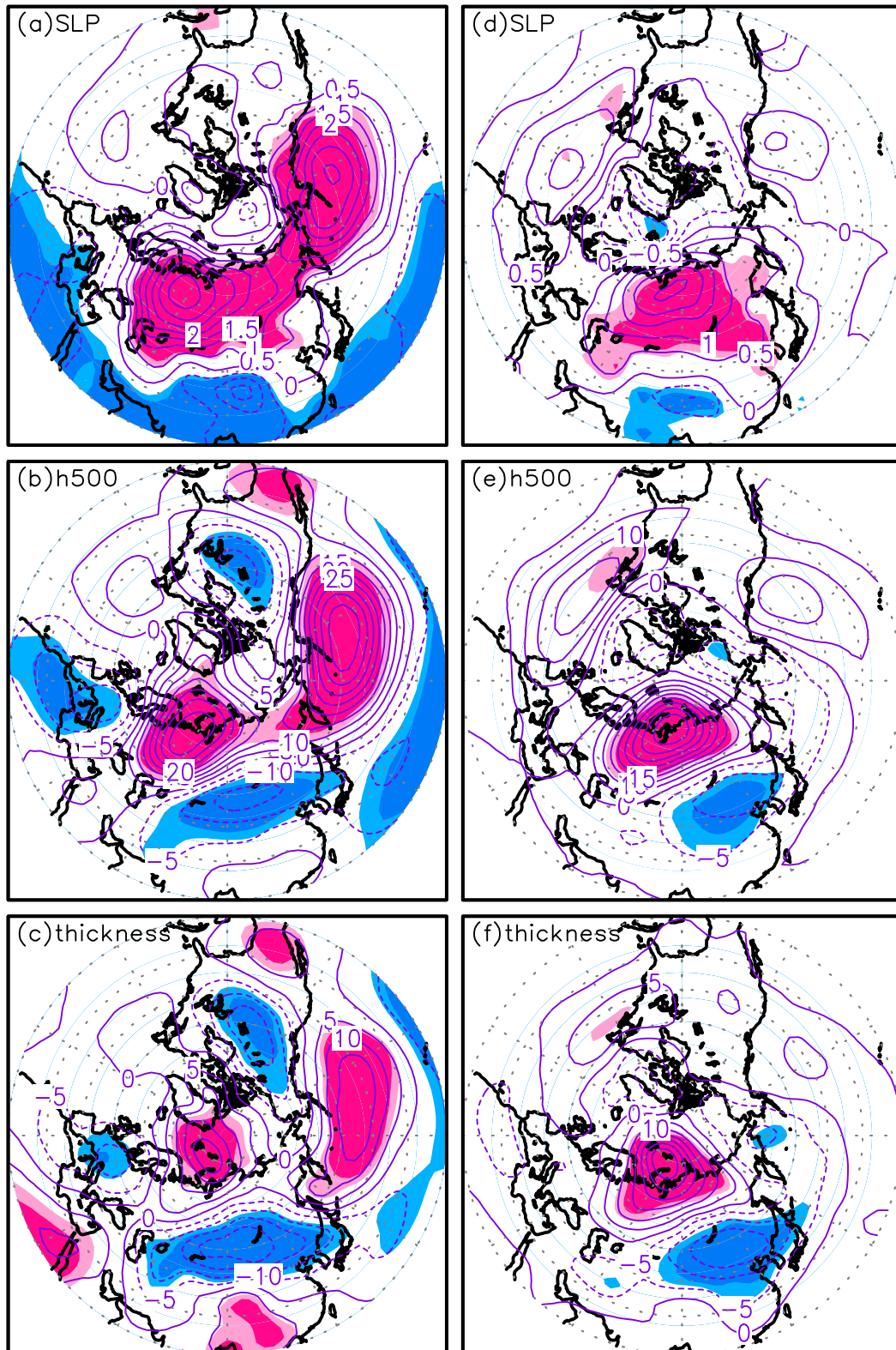


FIG. 5. Winter mean (a) SLP, (b) 500-hPa geopotential height, and (c) 1000–500-hPa thickness anomalies, derived from a linear regression on the normalized intensity index of the atmospheric circulation anomaly. (d)–(f) As in (a)–(c), but for derived from a linear regression on the detrended winter mean SAT index over the Barents–Kara Seas (70°–80°N, 30°–70°E; see [Kug et al. 2015](#)). The shading represents anomalies at the 95% (light) and 99% (dark) significance levels; contour intervals are 0.5 hPa in (a),(d) and 5 gpm in (b),(c),(e),(f).

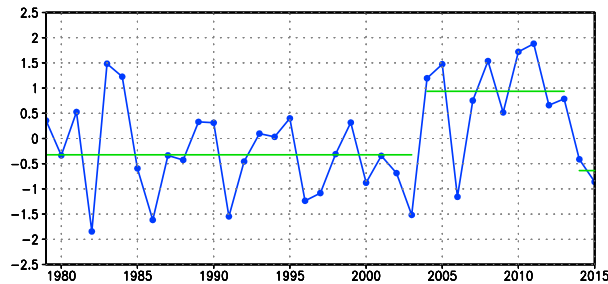


FIG. 6. The normalized intensity index of the atmospheric circulation anomaly (blue line) and means averaged over 1979/80–2003/04, 2004/05–2013/14, and 2014/15–2015/16 (green lines).

anomalies (Figs. 5c,f). Consequently, similar Arctic winter warm anomalies (Figs. 5c,f) can correspond to distinct large-scale circulation patterns.

b. Associations with previous atmospheric circulation patterns and the Siberian high

This atmospheric circulation anomaly differs from the Arctic Oscillation (AO) or the North Atlantic Oscillation (NAO). Figure 7 shows winter SLP anomalies corresponding to different EOF2 over different domains. This is a typical Arctic dipole anomaly shown in Fig. 7a, and opposing anomalous centers are located over the northern North America and the Siberian marginal seas and northern Eurasia (Wu et al. 2006). Additionally, there are two positive subcenters over the northeastern North Pacific and the northern North Atlantic. With the domain enlarging, although spatial distributions of SLP anomalies exhibit some similarities differences are also visible; for example, the extent with negative anomalies retreats and becomes weaker when the domain enlarges to south of 50°N. In contrast, positive anomalies in the middle and high latitudes, particularly from Eurasia eastward to the west coast of North America, are further enhanced (Figs. 7b–f). Additionally, over the domains south of 60°N, a center of positive SLP anomalies is steadily maintained around the Ural Mountains (Figs. 7c–f), differing from the Arctic dipole anomaly. Over the domains south of 70°N, winter SLP anomalies are no longer a dipole structure although there are significant correlations between the Arctic dipole anomaly and the second principal component (PC2) over different domains north of 30°N (Table 1). Additionally, correlations of the Arctic dipole anomaly with the PC2 rapidly decline from north of 60°N to north of 50°N. Consequently, the Arctic dipole anomaly is a “local” pattern north of 60°N. This atmospheric circulation anomaly is significantly correlated with the PC2 of EOF analysis of winter SLP variability over different domains only except for north of 70°N

where the correlation is not significant (Table 2). Consequently, this atmospheric circulation anomaly is different from the Arctic dipole anomaly and displays a closer association with atmospheric variability over the middle and lower latitudes relative to the Arctic. It seems like that this atmospheric circulation anomaly, to some extent, reflects a combination of two known wave trains: the Eurasian pattern and the PNA pattern. Their correlation coefficients are -0.52 (with the PNA pattern) and -0.63 (with the Eurasian pattern), respectively. It is also significantly correlated with the SHI ($r = 0.64$), further supporting that winter warm anomalies in the Arctic tend to be associated with a strengthened Siberian high (SH) (Kug et al. 2015). As shown in our previous study (Feng and Wu 2015), a strengthened SH and/or northward extended SH enhances cold air outflow from the Arctic into Asia; meanwhile, it also puts European warmer air inflow into the Arctic. Thus, a strengthened Eurasian cold high can be a conveyor and dynamically responsible for the warm Arctic–cold Eurasian pattern (Fig. 5c). Similarly, a weakened Aleutian low results in a cold North America and warm North Pacific. This atmospheric circulation anomaly significantly increases (decreases) frequencies of extreme cold events in Eurasia, the western North Pacific, and western North America (the Arctic and the area from the Okhotsk Sea to the North Pacific) (Fig. 8a), dynamically consistent with the spatial distribution of 500-hPa geopotential height anomalies in Fig. 5c. Figure 8b displays a regionally averaged frequency of extreme cold events in the central and eastern Eurasia. Before the winter of 2004/05, the mean frequency was below 13 times except for winters of 1983/84, 1984/85, and 1995/96 when their frequencies were close to or exceeding the mean value averaged over the period of recent Arctic winter warm anomalies. For this particular region, frequencies of extreme cold events mainly are controlled by the atmospheric circulation anomaly (Fig. 6).

c. Possible associations with Arctic SICs and SSTs

A further analysis shows that this atmospheric circulation anomaly is closely associated with both Arctic sea ice and SST in the previous autumn (Fig. 9). Statistically, the positive phase of this atmospheric circulation anomaly corresponds to negative anomalies in autumn SIC from the Barents Sea counterclockwise to the Beaufort Sea, particularly in the Barents–Kara Seas and the Pacific sector of the Arctic Ocean where significant negatively SIC anomalies are observed (Fig. 9a). This association is supported in observations and simulation experiments forced by Arctic SIC forcing (Wu et al. 2013a, and many others), which showed that decreased

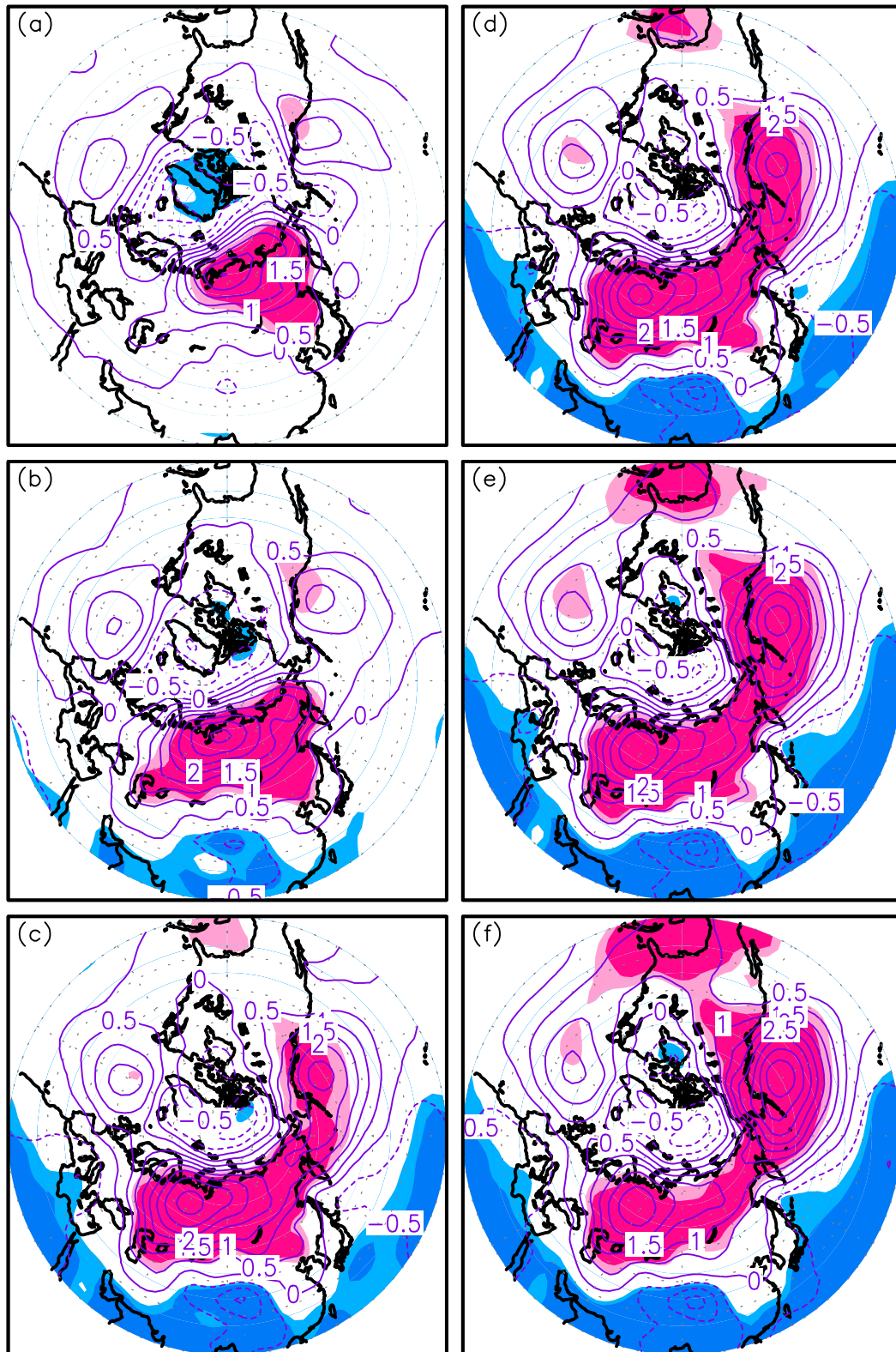


FIG. 7. Winter SLP anomalies, derived from a linear regression on the normalized PC2 time series over different domains, and the shading represents SLP anomalies at the 95% (light) and 99% (dark) significance levels: north of (a) 70°, (b) 60°, (c) 50°, (d) 40°, (e) 30°, and (f) 20°N.

TABLE 1. Correlation coefficients between the Arctic dipole anomaly and the PC2 of EOF analysis of winter SLP variability over different domains. Asterisks indicate correlations at the 95% significance level.

		North of			
	60°N	50°N	40°N	30°N	20°N
60°N	0.88*	0.56*	0.51*	0.43*	0.32

autumn Arctic SIC would strengthen winter SLP over the middle and high latitudes of Eurasia and produce a tripole structure in 500-hPa geopotential height anomalies closely resembling the Eurasian pattern. [Close et al. \(2015\)](#) investigated the timing of onset of rapid decline in Arctic SIC and showed that in the Barents–Kara Seas, the time of onset of rapid decline in autumn SIC is 2003 (see their Fig. 3b), consistent with recent Arctic winter warm anomalies since the winter of 2004/05 ([Fig. 1](#)).

Autumn SST anomalies display a negative phase of the PDO and significant negative SST anomalies in the tropical central and eastern Pacific and northeastern North Pacific ([Fig. 9b](#)). The correlations of this atmospheric circulation anomaly with autumn and winter PDO indices, however, are moderate (-0.37 and -0.42 , respectively) for the study period, mainly because of the PDO reflecting the background of SST anomalies. This result is basically consistent with [Screen and Francis \(2016\)](#), and they investigated the role of the PDO in resulting winter Arctic amplification and suggested that Arctic warming in response to sea ice decline is greater (reduced) during periods of the negative (positive) PDO phase. This atmospheric circulation anomaly displays a closer relationship with SST in the tropical central and eastern Pacific relative to the PDO, and the correlation with autumn (winter) Niño-3.4 index is -0.49 (-0.54). Thus, this atmospheric circulation anomaly links Arctic winter warm anomalies to SST cooling in the tropical central and eastern Pacific. A regionally averaged autumn SST in 0° – 14° N, 140° – 170° W can be regarded as a potential precursor to predict occurrences of this atmospheric circulation anomaly (their correlation is -0.56 ; [Fig. 9c](#)). Indeed, how autumn SST influences this atmospheric circulation anomaly and their possible linking mechanism deserves further investigation in the future. The result here implies that through affecting the atmospheric circulation anomaly, SST cooling in the tropical Pacific contributes to Arctic winter warm anomalies.

4. Conclusions

This study investigates dominant features of recent Arctic winter warm anomalies in the middle and lower

TABLE 2. Correlation coefficients with the PC2 of EOF analysis of winter SLP variability over different domains. Asterisks indicate correlations at the 95% significance level.

		North of				
	70°N	60°N	50°N	40°N	30°N	20°N
70°N	0.30	0.63*	0.87*	0.91*	0.90*	0.85*

troposphere and its association with winter atmospheric circulation anomalies. Results show that since the winter of 2004/05 winter Arctic atmosphere in the middle and lower troposphere has shifted to a warmer stage relative to the winter mean averaged from 1979/80 to 2003/04. Meanwhile, positive SLP anomalies are observed in the middle and high latitudes of Eurasia, the Siberian marginal seas of the Arctic Ocean, and the North Pacific, and negative SLP anomalies occupy the low latitudes from Africa eastward to the central Pacific.

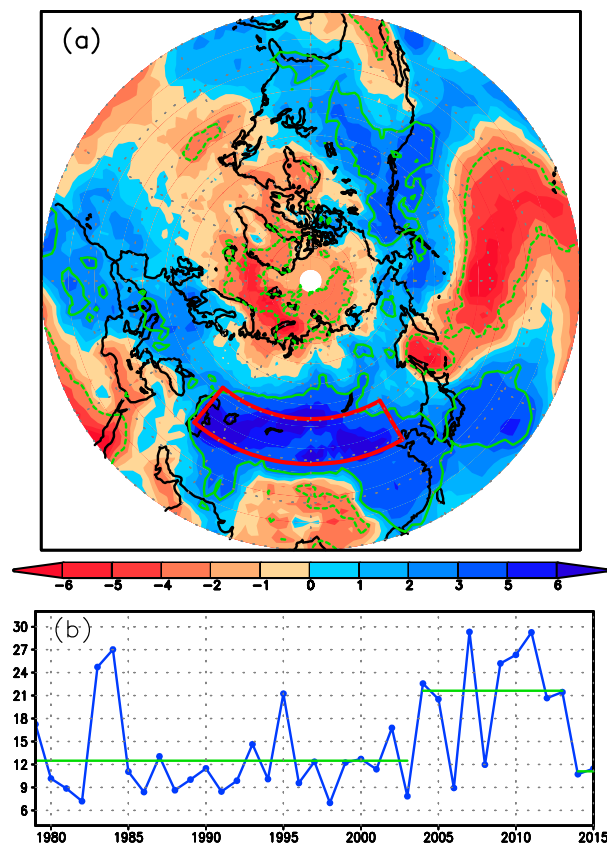


FIG. 8. (a) Regression map of accumulative frequencies of winter daily extreme cold events, regressed on the normalized intensity index of the atmospheric circulation anomaly, and the area surrounded by the green contours represents anomalous frequencies at the 95% significance level. (b) Time series of the regionally averaged accumulative winter daily extreme cold events from the area outlined in red in (a).

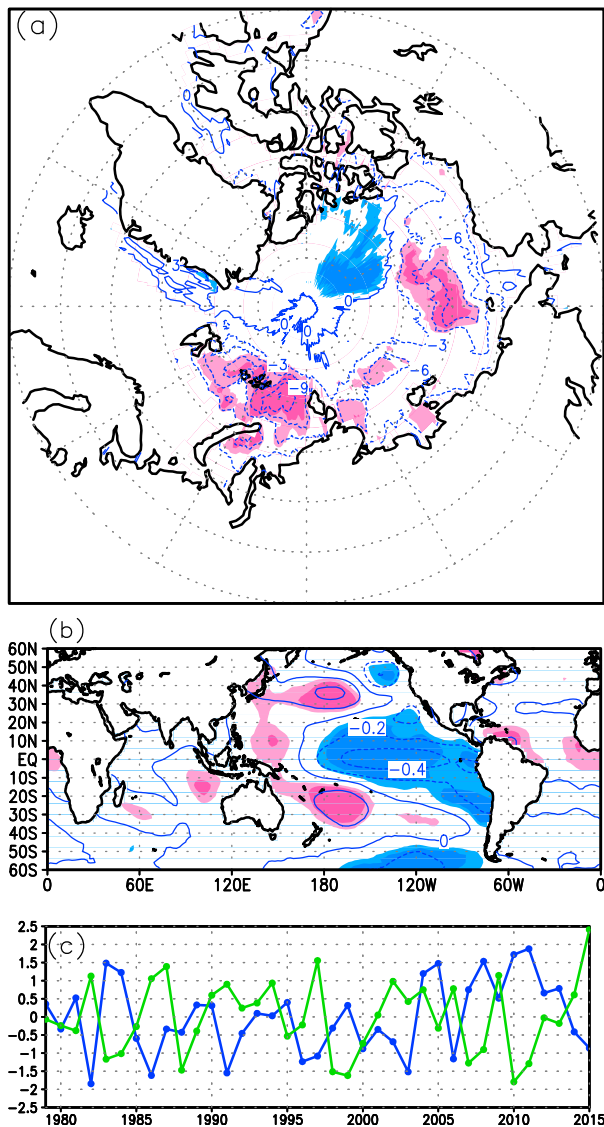


FIG. 9. (a) Autumn SIC anomalies, derived from a linear regression on the normalized intensity index of the atmospheric circulation anomaly; the shading denotes SIC anomalies at the 95% (light) and 99% (dark) significance levels, and the contour interval is 3%. (b) As in (a), but for autumn SST anomalies; contour interval is 0.2°C . (c) The normalized intensity index of the atmospheric circulation anomaly (blue line) and the regionally averaged autumn SST (green line) for $0^{\circ}\text{--}14^{\circ}\text{N}$, $140^{\circ}\text{--}170^{\circ}\text{W}$; their correlation is -0.56 .

Correspondingly, winter 500-hPa geopotential height anomalies display wave train structures over Eurasia, the North Pacific, and North America.

These major features frequently reappear during recent Arctic winter warm anomalies. A regionally averaged winter SLP in $40^{\circ}\text{--}65^{\circ}\text{N}$, $30^{\circ}\text{E--}150^{\circ}\text{W}$ can be regarded as the intensity index to characterize interannual variability of the atmospheric circulation anomaly associated with recent Arctic winter warm anomalies. The

positive phase of this atmospheric circulation anomaly corresponds to warm anomalies over the Arctic, the North Pacific, northern Africa, and the low latitudes of both North American and Asian continents, with cold anomalies in Europe, the middle and high latitudes of Asia, and North America. Correspondingly, winter 500-hPa geopotential height anomalies combine some major characteristics of both the PNA and Eurasian patterns, and three positive anomalous centers are respectively located over northern Eurasia close to the Barents–Kara Seas, the North Pacific, and southern United States, with three negative centers over Europe and the middle and high latitudes of Asia and North America. This atmospheric circulation anomaly is different from the Arctic dipole anomaly and displays a closer association with atmospheric variability over the middle and low latitudes relative to the Arctic. It directly connects Arctic warm anomalies in the middle and lower troposphere to increased frequencies of extreme cold events in Eurasia, the western North Pacific, and western North America, with decreased frequencies of extreme cold events in the Arctic and from the Okhotsk Sea to the North Pacific. Results also imply that in addition to Arctic sea ice loss, SST cooling in the tropical central and eastern Pacific may contribute to recent Arctic winter warm anomalies, although its relative contributions and impact mechanism are still unclear.

Acknowledgments. The authors are grateful to the anonymous reviewers for their constructive and helpful comments. This study was supported by the National Key Basic Research Project of China (2015CB453200) and the National Natural Science Foundation of China (41475080 and 41661144017).

REFERENCES

- Andry, O., R. Bintanja, and W. Hazeleger, 2017: Time-dependent variations in the Arctic's surface albedo feedback and the link to seasonality in sea ice. *J. Climate*, **30**, 393–410, doi:10.1175/JCLI-D-15-0849.1.
- Barnes, E., 2013: Revisiting the evidence linking Arctic amplification to extreme weather in midlatitudes. *Geophys. Res. Lett.*, **40**, 4734–4739, doi:10.1002/grl.50880.
- , and J. Screen, 2015: The impact of Arctic warming on the midlatitude jet-stream: Can it? Has it? Will it? *Wiley Interdiscip. Rev.: Climate Change*, **6**, 277–286, doi:10.1002/wcc.337.
- Close, S., M.-N. Houssais, and C. Herbaut, 2015: Regional dependence in the timing of onset of rapid decline in Arctic sea ice concentration. *J. Geophys. Res. Oceans*, **120**, 8077–8098, doi:10.1002/2015JC011187.
- Cohen, J., 2016: An observational analysis: Tropical relative to Arctic influence on midlatitude weather in the era of Arctic amplification. *Geophys. Res. Lett.*, **43**, 5287–5294, doi:10.1002/2016GL069102.

- , J. Furtado, M. Barlow, V. Alexeev, and J. Cherry, 2012: Arctic warming, increasing snow cover and widespread boreal winter cooling. *Environ. Res. Lett.*, **7**, 014007, doi:10.1088/1748-9326/7/1/014007.
- , and Coauthors, 2014: Recent Arctic amplification and extreme mid-latitude weather. *Nat. Geosci.*, **7**, 627–637, doi:10.1038/ngeo2234.
- Feng, C., and B. Wu, 2015: Enhancement of winter Arctic warming by the Siberian high over the past decade. *Atmos. Ocean. Sci. Lett.*, **8**, 257–263, doi:10.3878/AOSL20150022.
- Francis, J., and S. Vavrus, 2012: Evidence linking Arctic amplification to extreme weather in mid-latitudes. *Geophys. Res. Lett.*, **39**, L06801, doi:10.1029/2012GL051000.
- , and —, 2015: Evidence for a wavier jet stream in response to rapid Arctic warming. *Environ. Res. Lett.*, **10**, 014005, <https://doi.org/10.1088/1748-9326/10/1/014005>.
- Hadley Centre for Climate Prediction and Research, 2006: Met Office HadISST 1.1-Global sea-ice coverage and Sea Surface Temperature (1870-2015). NCAS British Atmospheric Data Centre, accessed 21 April 2017, <http://catalogue.ceda.ac.uk/uuid/facafa2ae494597166217a9121a62d3c>.
- Jaiser, R., K. Dethloff, D. Handorf, A. Rinke, and J. Cohen, 2012: Impact of sea ice cover changes on the Northern Hemisphere atmospheric winter circulation. *Tellus*, **64A**, 11595, doi:10.3402/tellusa.v64i0.11595.
- Jung, T., and Coauthors, 2015: Polar-lower latitude linkages and their role in weather and climate prediction. *Bull. Amer. Meteor. Soc.*, **96**, ES197–ES200, doi:10.1175/BAMS-D-15-00121.1.
- Kug, J., J. Jeong, Y. Jang, B. Kim, C. Folland, S. Min, and S. Son, 2015: Two distinct influences of Arctic warming on cold winters over North America and East Asia. *Nat. Geosci.*, **8**, 759–762, doi:10.1038/ngeo2517.
- Overland, J., and M. Wang, 2010: Large-scale atmospheric circulation changes are associated with the recent loss of Arctic sea ice. *Tellus*, **62A**, 1–9, doi:10.1111/j.1600-0870.2009.00421.x.
- , K. Wood, and M. Wang, 2011: Warm Arctic–cold continents: Climate impacts of the newly open Arctic sea. *Polar Res.*, **30**, 15787, doi:10.3402/polar.v30i0.15787.
- , J. Francis, R. Hall, E. Hanna, S. Kim, and T. Vihma, 2015: The melting Arctic and midlatitude weather patterns: Are they connected? *J. Climate*, **28**, 7917–7932, doi:10.1175/JCLI-D-14-00822.1.
- , and Coauthors, 2016: Nonlinear response of mid-latitude weather to the changing Arctic. *Nat. Climate Change*, **6**, 992–999, doi:10.1038/nclimate3121.
- Perlwitz, J., M. Hoerling, and R. Dole, 2015: Arctic tropospheric warming: Causes and linkages to lower latitudes. *J. Climate*, **28**, 2154–2167, doi:10.1175/JCLI-D-14-00095.1.
- Petoukhov, V., and V. Semenov, 2010: A link between reduced Barents–Kara sea ice and cold winter extremes over northern continents. *J. Geophys. Res.*, **115**, D21111, doi:10.1029/2009JD013568.
- Screen, J., and I. Simmonds, 2010: The central role of diminishing sea ice in recent Arctic temperature amplification. *Nature*, **464**, 1334–1337, doi:10.1038/nature09051.
- , and —, 2013: Exploring links between Arctic amplification and mid-latitude weather. *Geophys. Res. Lett.*, **40**, 959–964, doi:10.1002/grl.50174.
- , and J. Francis, 2016: Contribution of sea-ice loss to Arctic amplification is regulated by Pacific Ocean decadal variability. *Nat. Climate Change*, **6**, 856–860, doi:10.1038/nclimate3011.
- , C. Deser, I. Simmonds, and R. Tomas, 2014: Atmospheric impacts of Arctic sea-ice loss, 1979–2009: Separating forced change from atmospheric internal variability. *Climate Dyn.*, **43**, 333–344, doi:10.1007/s00382-013-1830-9.
- Sellevold, R., S. Sobolowski, and C. Li, 2016: Investigating possible Arctic–midlatitude teleconnections in a linear framework. *J. Climate*, **29**, 7329–7343, doi:10.1175/JCLI-D-15-0902.1.
- Semenov, A., and M. Latif, 2015: Nonlinear winter atmospheric circulation response to Arctic sea ice concentration anomalies for different periods during 1966–2012. *Environ. Res. Lett.*, **10**, 054020, doi:10.1088/1748-9326/10/5/054020.
- Serreze, M., and R. Barry, 2011: Processes and impacts of Arctic amplification: A research synthesis. *Global Planet. Change*, **77**, 85–96, doi:10.1016/j.gloplacha.2011.03.004.
- Smith, T., and R. Reynolds, 2003: Extended reconstruction of global sea surface temperature based on COADS data (1854–1997). *J. Climate*, **16**, 1495–1510, doi:10.1175/1520-0442-16.10.1495.
- Sun, L., J. Perlwitz, and M. Hoerling, 2016: What caused the recent “warm Arctic, cold continents” trend pattern in winter temperatures? *Geophys. Res. Lett.*, **43**, 5345–5352, doi:10.1002/2016GL069024.
- Vihma, T., 2014: Effects of Arctic sea ice decline on weather and climate: A review. *Surv. Geophys.*, **35**, 1175–1214, <https://doi.org/10.1007/s10712-014-9284-0>.
- Wallace, J., I. Held, D. Thompson, K. Trenberth, and J. Walsh, 2014: Global warming and winter weather. *Science*, **343**, 729–730, doi:10.1126/science.343.6172.729.
- Walsh, J. E., 2014: Intensified warming of the Arctic: Causes and impacts on middle latitudes. *Global Planet. Change*, **117**, 52–63, doi:10.1016/j.gloplacha.2014.03.003.
- Wu, B., and J. Wang, 2002: Winter Arctic Oscillation, Siberian high and East Asian winter monsoon. *Geophys. Res. Lett.*, **29**, 1897, doi:10.1029/2002GL015373.
- , —, and J. Walsh, 2006: Dipole Anomaly in the winter Arctic atmosphere and its association with sea ice motion. *J. Climate*, **19**, 210–225, doi:10.1175/JCLI3619.1.
- , D. Handorf, K. Dethloff, A. Rinke, and A. Hu, 2013a: Winter weather patterns over northern Eurasia and Arctic sea ice loss. *Mon. Wea. Rev.*, **141**, 3786–3800, doi:10.1175/MWR-D-13-00046.1.
- , R. Zhang, R. D’Arrigo, and J. Su, 2013b: On the relationship between winter sea ice and summer atmospheric circulation over Eurasia. *J. Climate*, **26**, 5523–5536, doi:10.1175/JCLI-D-12-00524.1.
- , J. Su, and R. D’Arrigo, 2015: Patterns of Asian winter climate variability and links to Arctic sea ice. *J. Climate*, **28**, 6841–6858, doi:10.1175/JCLI-D-14-00274.1.